

RESEARCH ARTICLE

Prediction of the Time Course of Callus Stiffness as a Function of Mechanical Parameters in Experimental Rat Fracture Healing Studies - A Numerical Study

Tim Wehner, Malte Steiner*, Anita Ignatius, Lutz Claes

Institute of Orthopedic Research and Biomechanics, Center of Musculoskeletal Research Ulm, University Hospital Ulm, Ulm, Germany

*malte.steiner@uni-ulm.de



CrossMark
click for updates

 OPEN ACCESS

Citation: Wehner T, Steiner M, Ignatius A, Claes L (2014) Prediction of the Time Course of Callus Stiffness as a Function of Mechanical Parameters in Experimental Rat Fracture Healing Studies - A Numerical Study. PLoS ONE 9(12): e115695. doi:10.1371/journal.pone.0115695

Editor: Christof Markus Aegerter, University of Zurich, Switzerland

Received: August 13, 2014

Accepted: November 26, 2014

Published: December 22, 2014

Copyright: © 2014 Wehner et al. This is an open-access article distributed under the terms of the [Creative Commons Attribution License](https://creativecommons.org/licenses/by/4.0/), which permits unrestricted use, distribution, and reproduction in any medium, provided the original author and source are credited.

Data Availability: The authors confirm that all data underlying the findings are fully available without restriction. All relevant data are within the paper and its Supporting Information files.

Funding: This work was funded by the German Research Foundation (WE 4859/1-1), www.dfg.de. The funders had no role in study design, data collection and analysis, decision to publish, or preparation of the manuscript.

Competing Interests: The authors have declared that no competing interests exist.

Abstract

Numerous experimental fracture healing studies are performed on rats, in which different experimental, mechanical parameters are applied, thereby prohibiting direct comparison between each other. Numerical fracture healing simulation models are able to predict courses of fracture healing and offer support for pre-planning animal experiments and for post-hoc comparison between outcomes of different *in vivo* studies. The aims of this study are to adapt a pre-existing fracture healing simulation algorithm for sheep and humans to the rat, to corroborate it using the data of numerous different rat experiments, and to provide healing predictions for future rat experiments. First, material properties of different tissue types involved were adjusted by comparing experimentally measured callus stiffness to respective simulated values obtained in three finite element (FE) models. This yielded values for Young's moduli of cortical bone, woven bone, cartilage, and connective tissue of 15,750 MPa, 1,000 MPa, 5 MPa, and 1 MPa, respectively. Next, thresholds in the underlying mechanoregulatory tissue differentiation rules were calibrated by modifying model parameters so that predicted fracture callus stiffness matched experimental data from a study that used rigid and flexible fixators. This resulted in strain thresholds at higher magnitudes than in models for sheep and humans. The resulting numerical model was then used to simulate numerous fracture healing scenarios from literature, showing a considerable mismatch in only 6 of 21 cases. Based on this corroborated model, a fit curve function was derived which predicts the increase of callus stiffness dependent on bodyweight, fixation stiffness, and fracture gap size. By mathematically predicting the time course of the healing process prior to the animal studies, the data presented in this work provides support for planning new fracture healing experiments in rats. Furthermore, it allows one to

transfer and compare new *in vivo* findings to previously performed studies with differing mechanical parameters.

Introduction

The rat is of particular importance for experimental studies in fracture healing. The outcome of the healing process is often evaluated via determination of the callus stiffness by *ex vivo* mechanical testing at certain healing time points [1, 2, 3, 4, 5]. Mechanical and biological factors influence the manner in which fracture healing progresses [6, 7, 8]. The most important mechanical factor is the interfragmentary movement (IFM) [6]; IFM determines the tissue strains at the fracture site in relation to the fracture gap size and regulates the mechanically induced tissue differentiation [9, 10]. The IFM depends on the fixation stability and the musculoskeletal loads which are primarily dependent on the bodyweight of the animals [11]. Therefore, experimental studies in rats are not directly comparable with each other when different experimental parameters (bodyweight, fixation stiffness, fracture gap size) are used.

Over the last decade, several numerical models for simulating the fracture healing process were developed [12, 13, 14, 15, 16, 17, 18]. Those models, which take the experimental parameters mentioned above into consideration, have the potential to simulate the healing process prior to an *in vivo* investigation helping to refine and reduce the number of animals in experimental studies as well as provide comparability between different studies by appropriate pre-experiment planning. Furthermore, simulations can be used to normalize already published *in vivo* results by simulating the healing process with the specific set of experimental parameters. Thereby, they help decide if there is an interesting biological factor influencing the healing outcome or if the differences of the healing outcome between studies can be explained solely by mechanical parameters that influence tissue strains (fixation stiffness, bodyweight, fracture geometry).

The aims of this study were (a) to adapt an existing numerical algorithm that reasonably simulates fracture healing in sheep [18, 19] and in humans [20, 21] to the conditions found in rats, which includes the determination of callus tissue properties and the calibration of the underlying mechanoregulatory tissue differentiation rules, (b) to simulate *in vivo* studies from literature and evaluate their agreement and (c) to predict the time course of the callus stiffness under several combinations of fixation stability, bodyweight, and fracture geometry. For future fracture healing studies using rats, this should promote the replacement of experimental *in vivo* studies, and allow focus on the influence of biological factors.

Methods

Determining the material properties of the callus tissues

To determine the material properties of the different callus tissues involved (*i.e.* connective tissue, cartilage, woven and cortical bone), three FE models of different healing stages were created in ANSYS 14.0 (ANSYS Inc., Canonsburg, PA, USA) to calculate the respective callus bending stiffness. All geometries represented transverse osteotomies at the rat femur in accordance with [Fig. 1](#): (1) intact bone cylinder, (2) callus filled with woven bone according to previous histological findings under rigid fixation after 35 days of healing [\[2\]](#), (3) callus filled with woven bone except within the fracture gap, which was filled with cartilage (periosteal callus) and connective tissue (endosteal callus) according to previous histological findings under flexible fixation after 35 days of healing [\[2\]](#). Conforming to [Checa et al. \[22\]](#), the cortical bones were modeled as hollow cylinders with an inner diameter of 2 mm and an outer diameter of 4 mm. The overall height (l) of the models was 24 mm. All structures were meshed with 10-node tetrahedral elements assuming linear-elastic, isotropic material properties. The models were fixed at the bottom (distal end of the distal cortical bone fragment) in all degrees of freedom. To simulate the bending stiffness of the models in a cantilever bending mode, a shear deflection of 1 mm was applied to the top of the models. Therefore, a tent-like structure made of rigid beam elements [\[21\]](#) was used at the top of the models to allow the application of the shear deflection U_s and the calculation of the reaction force F_s at one single node. The bending stiffness, EI_{FE} , was calculated based on the formula for cantilever bending:

$$EI_{FE} = \frac{F_s l^3}{U_s 3} \quad (1)$$

These three FE models were used to successively obtain the material properties by comparing the simulated bending stiffness EI_{FE} , resulting from various parameter combinations to the respective *ex vivo* bending stiffness EI_{EX} measured in rat experiments by [Recknagel et al. \[2\]](#) Thus, model (1) was used to obtain Young's modulus for cortical bone E_{cort} , which was then assigned to model (2). This was then used to obtain Young's modulus for woven bone E_{bone} , which subsequently was assigned to model (3), to obtain Young's moduli for endosteal callus $E_{endoste}$ and gap tissue E_{gap} , as listed in the supporting information (cf. [S1 Table](#)).

Numerical simulation of the fracture healing process

To simulate the fracture healing process, the previously obtained material properties were assigned to another callus FE model with an ellipsoid shaped healing region with an outer diameter of 10 mm, which allowed a maximum callus index [\[23\]](#) (ratio between the outer callus diameter and the periosteal diameter of the cortices) of 2.5. The external fixator and the fixator pins were

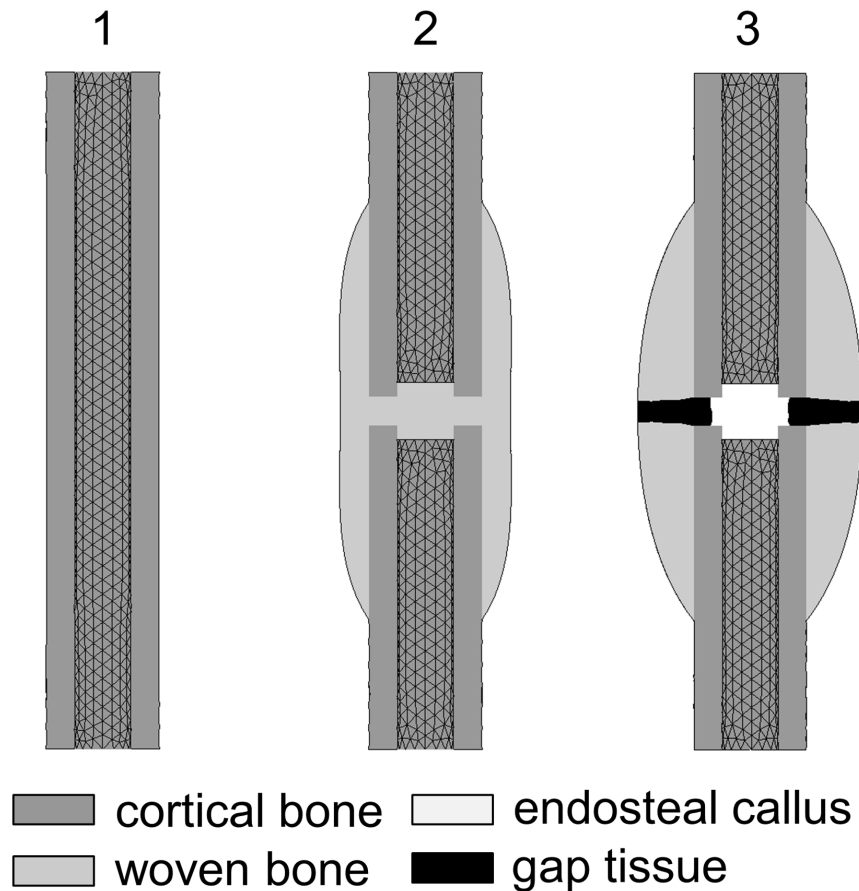


Fig. 1. Three finite element models for bending stiffness calculation of three different healing scenarios. Model 1: intact bone cylinder, model 2: fracture callus filled with woven bone and a callus index of 1.5, and model 3: fracture callus with a callus index of 2, where periosteal callus is filled with woven bone up to the fracture line.

doi:10.1371/journal.pone.0115695.g001

modeled with 2-node beam elements with six degrees of freedom at each node, allowing the simulation of various fixation stabilities by changing the free bending length (offset) of the pins. The model was fixed at the end near the fracture gap of the distal cortical bone fragment in all degrees of freedom. A three dimensional physiological load case (three forces and three moments at that time point during gait of the rats when the axial load component reached its maximum, which was 6 times bodyweight [11]) was applied to the proximal cortical bone fragment using a tent like construct at the end of the proximal cortical bone fragment at the fracture site [21]. The fracture healing process was simulated iteratively over the healing time [18, 19, 21]. At each simulation step, an FE-simulation was performed to calculate the local mechanical stimuli (volumetric strain ϵ_v and distortional strain ϵ_d) and subsequently predict the change in the local tissue distribution within the elements of the healing region. Last, Young's modulus (E_{tiss}) and Poisson's ratio (ν_{tiss}) of the FE were updated according to the new tissue composition, *i.e.* the concentration of cartilage (c_{cart}) and bone (c_{bone}), using

the following rules of mixtures:

$$E = E_{conn} + c_{cart}^3(E_{cart} - E_{conn}) + c_{bone}^3(E_{bone} - E_{conn}) \quad (2)$$

$$\nu = \nu_{conn}c_{conn} + \nu_{cart}c_{cart} + \nu_{bone}c_{bone}, \quad (3)$$

where E_{conn} , ν_{conn} , E_{cart} , ν_{cart} , and E_{bone} , ν_{bone} , are Young's moduli and Poisson's ratios of connective tissue, cartilage, and woven bone, respectively.

In contrast to previous simulations of this research group [18, 19, 21, 24], the complexity of the rules for predictions of the tissue differentiation was reduced. Now, bone and cartilage formation were directly linked solely to the mechanical stimuli (ε_v & ε_d). Cartilage formation was allowed for volumetric strains in the range of $\varepsilon_{v, cart, low} < \varepsilon_v < \varepsilon_{v, cart, high}$ in combination with distortional strains in the range of $\varepsilon_{d, cart, low} < \varepsilon_d < \varepsilon_{d, cart, high}$, whereas bone formation was allowed in the range of the volumetric strains of $\varepsilon_{v, bone, low} < \varepsilon_v < \varepsilon_{v, bone, high}$ in combination with distortional strains in the range of $\varepsilon_{d, bone, low} < \varepsilon_d < \varepsilon_{d, bone, high}$. Outside these ranges, resorption of these tissues will occur (cf. Fig. 2).

To simulate bone and cartilage formation and resorption, the rate of change in both concentrations was set to 7% per day, since this allowed simulation of a bony callus after 35 days of healing with a size according to previous findings [2].

Calibration of the underlying mechanoregulatory rules

To adapt the fracture healing algorithm from sheep to rat, the thresholds within the underlying mechanoregulatory tissue differentiation rules (*i.e.* $\varepsilon_{v, cart, low}$, $\varepsilon_{v, cart, high}$, $\varepsilon_{d, cart, high}$, and $\varepsilon_{d, bone, high}$, cf. Fig. 2) were varied in 600 different combinations (designs) in a design of experiments (DOE) approach using Latin Hypercube Sampling in the software package optiSLang (Dynardo GmbH, Weimar, Germany). The other parameters defining the ranges of the mechanical stimuli were kept constant to the following values: $\varepsilon_{v, bone, low} = \varepsilon_{v, cart, high}$, $\varepsilon_{v, bone, high} = -\varepsilon_{v, cart, high}$, $\varepsilon_{d, cart, low} = 0$, $\varepsilon_{d, bone, low} = 1000 \mu\varepsilon$ [25]. The simulations were performed according to the experimental setup of a previously published *in vivo* monitoring study [26]: the fracture healing process was simulated for each design under rigid ($K_{ax} = 102$ N/mm) and flexible ($K_{ax} = 30$ N/mm) fixation and the callus stiffness was calculated at each week until 6 weeks (for rigid fixation), or 12 weeks (for flexible fixation). The mean values of differences between simulated and their respective *in vivo* measured callus stiffness were calculated and used to find the best design out of the 600.

Evaluation and corroboration of the numerical fracture healing model

To evaluate the validity of the calibrated fracture healing algorithm, it was used to simulate 21 *in vivo* scenarios from 9 different experimental rat fracture healing

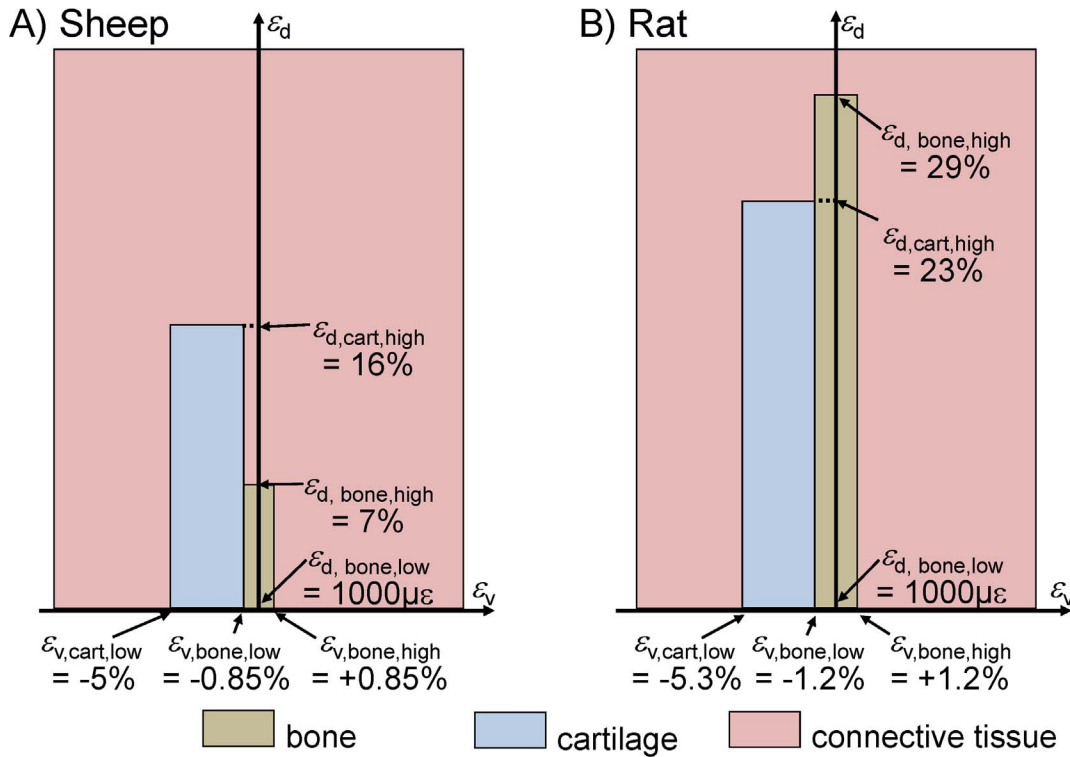


Fig. 2. Mechanoregulatory hypothesis for tissue differentiation dependent on the local volumetric (ϵ_v) and distortional (ϵ_d) strains. A) Established for sheep, according to Claes and Heigele [9], B) for rat after calibration of the model in the present study.

doi:10.1371/journal.pone.0115695.g002

studies from literature (Table 1). Simulation outcomes (*i.e.* simulated callus stiffness) were compared to the *ex vivo* callus stiffness from the respective experiment. Requirements for the included *in vivo* studies were transverse osteotomies of rat femurs, stabilization with external fixators with well described experimental parameters (bodyweight of the animals, fixation stiffness and fracture gap size), and well reported *ex vivo* mechanical testing of the callus stiffness.

Prediction of callus stiffness subject to bodyweight, fixation stiffness and fracture gap size

For numerous combinations of different values for bodyweight (BW), fixation stability (K_{ax}), and fracture gap size (S_{fr}), fracture healing was simulated with the calibrated and corroborated iterative algorithm described above. For each iteration step, the callus bending stiffness K_C was calculated by simulating a cantilever bending test. For these time courses of K_C , fit curves with a sigmoidal shape were created using the Curve Fitting Toolbox of Matlab (MathWorks, Ismaning, Germany) with the equation

Table 1. Literature data of different rat experiments which measured the *ex vivo* callus stiffness ($K_{c,ex vivo}$) at healing time point t_H . $K_{c,sim}$ is the callus stiffness, obtained by numerical simulation applying the same bodyweight (BW), axial fixation stiffness (K_{ax}) and fracture gap size (S_{fr}) as the respective *in vivo* experiment.

Data set #	Reference	BW in g	gender (m or f)	K_{ax} in N/mm	S_{fr} in mm	t_H in days	$K_{c,ex vivo}$ in %	$K_{c,sim}$ in %
1	Harrison <i>et al.</i> [30]	500	m	46	0.5	63	189 ± 47	115
2	Harrison <i>et al.</i> [30]	500	m	46	3	63	n.a.	114
3	Mark <i>et al.</i> [5]	400	m	30	2	14	n.a.	2 (2)**
4	Mark <i>et al.</i> [5]	400	m	30	2	28	5 ± 1	7 (5)**
5	Mark <i>et al.</i> [5]	400	m	30	2	42	50 ± 18	95 (54)**
6	Mark <i>et al.</i> [5]	400	m	30	2	84	161 ± 9	114 (117)**
7	Kaspar <i>et al.</i> [32]	435	m	34	0.5	56	70–209	113
8	Strube <i>et al.</i> [3]	257	f	25	1.5	42	176 ± 38	100
9	Strube <i>et al.</i> [3]	257	f	10	1.5	42	78 ± 26	108
10	Strube <i>et al.</i> [3]	335	f	25	1.5	42	25 ± 9	107
11	Strube <i>et al.</i> [3]	335	f	10	1.5	42	38 ± 23	54
12	Strube <i>et al.</i> [4]	363	m	10	1.5	42	43–83*	29
13	Strube <i>et al.</i> [4]	353	f	10	1.5	42	16–44*	36
14	Claes <i>et al.</i> [1]	375	m	74	1	35	53 ± 10	100
15	Claes <i>et al.</i> [1]	375	m	10	1	35	35 ± 10	11
16	Mehta <i>et al.</i> [37]	366	m	25	1.5	42	52 ± 20	28
17	Mehta <i>et al.</i> [31]	326	m	50	1	42	90–132*	99
18	Mehta <i>et al.</i> [31]	326	m	50	5	56	0–15*	106
19	Mehta <i>et al.</i> [31]	296	f	50	1	42	50–107*	98
<i>Study used for adjusting the thresholds in the underlying mechanoregulatory rules:</i>								
20	Recknagel <i>et al.</i> [2]	425	m	119	1	35	31–82*	100
21	Recknagel <i>et al.</i> [2]	425	m	32	1	35	19–32*	19
<i>Study used for determining the fracture callus material properties:</i>								
–	Wehner <i>et al.</i> [26]	467	m	102	1	84	126	100
–	Wehner <i>et al.</i> [26]	467	m	30	1	84	106	100

*Interquartile range, **simulated with a bodyweight of 450 g.
 #1–2: develop a pseudarthrosis model with large fracture gap.
 #3–6: examine torsional callus stiffness over healing time.
 #7: develops a reproducible standardized rat bone healing model.
 #8–11: investigate mechanical impact on fracture healing in aged rats.
 #12–13: contribution of mesenchymal stem cells to sex-specific differences in bone healing.
 #14–15: investigate the influence of early dynamization on fracture healing.
 #16: examine the influence of gender and fixation stability on bone defect healing.
 #17–19: develop a reproducible atrophic non-union.
 #20–21: investigate how blunt chest trauma impairs fracture healing in rats.

doi:10.1371/journal.pone.0115695.t001

$$K_C = a \left(1 + e^{\frac{t_0 - t}{b}} \right)^{-1} \tag{4}$$

Using these fit curves, the time to heal (assumed as the time point when the callus stiffness reached 90% of the intact bone stiffness) was calculated for all of these cases and correlated to the initial IFM (defined as the axial internal force in

the femoral mid-shaft, which was assumed to be 6 times the bodyweight [11], divided by the axial fixation stiffness) and to the interfragmentary strain (defined as the IFM divided by the fracture gap size). Furthermore, the deviations (minimum Δ_{min} , median Δ_{median} and maximum Δ_{max}) of the resulting fit curve in comparison to the original simulated curves were calculated to allow evaluation of the fidelity of the fitting function.

Results

Determining the material properties of the callus tissues

Using a Young's modulus of 15,750 MPa for the cortical bone of the intact bone model (Fig. 1) led to a bending stiffness of 182,358 Nmm², which is in good accordance with the *ex vivo* bending stiffness of intact rat femurs ($176,805 \pm 51,586$ Nmm²), measured by Recknagel *et al.* [2]. Therefore, the material properties for the cortical shells were incorporated into models 2 and 3 (Fig. 1). Model 2, for the simulation of a callus filled with woven bone with a Young's modulus of 1,000 MPa, led to a bending stiffness of approx. 100% of the intact bones, typical for a fully bony bridged fracture callus with moderate callus size (callus index=1.5) [2, 27, 28]. Therefore, the woven bone in model 3 (Fig. 1) was assigned this value for Young's modulus. Model 3 (Fig. 1) represented a fracture callus with a greater size (callus index=2) and a fracture gap of 1 mm, filled with connective tissue and cartilage, typical for a healing situation after 35 days under a more flexible fixation [2]. Using a Young's modulus of 5 MPa for cartilage led to a bending stiffness of 28% to 29% of the intact bones, which is in good agreement with the *ex vivo* results ($25 \pm 11\%$) of Recknagel *et al.* [2]. The obtained material properties are summarized in Table 2.

Calibration of the underlying mechanoregulatory rules

The best agreement between *in vivo* data and simulations were obtained by shifting the threshold values of the underlying mechanoregulatory rules towards higher levels ($\epsilon_{v, cart, low} = -5.3\%$, $\epsilon_{v, cart, high} = -1.2\%$, $\epsilon_{d, cart, high} = 23\%$, and $\epsilon_{d, bone, high} = 29\%$, cf. Fig. 2B) in comparison to the thresholds that were used in previous simulations ($\epsilon_{v, cart, low} = -5\%$, $\epsilon_{v, cart, high} = -0.85\%$, $\epsilon_{d, cart, high} = 16\%$, and $\epsilon_{d, bone, high} = 7\%$, cf. Fig. 2A) for sheep and humans [18, 19, 21]. Applying these calibrated thresholds, the time course of the callus stiffness was predicted in good accordance with the *in vivo* data from the previous study [29] (Fig. 3). Regarding the tissue distribution after 35 days of healing, the simulations yield a bridged, bony callus of moderate size under rigid fixation (callus index approximately 1.5), and a larger bony callus (callus index approximately 2.0) under flexible fixation, with a remaining fracture gap that contains connective tissue and cartilage (Fig. 4). These predictions correspond well to respective, previous findings [2, 29].

Table 2. Material properties obtained for the simulated callus tissues.

Tissue type	Young's modulus in MPa	Poisson's ratio
Cortical bone	15,750 ^a	0.36 ^e
Woven bone	1,000 ^b	0.36 ^e
Cartilage	5 ^c	0.45 ^e
Granulation/connective tissue	1 ^d	0.4 ^e

^aSmit *et al.*, 2002 [35], obtained as isotropic elastic constant in a poroelastic material model.

^bCheca *et al.*, 2011 [22], used for the solid phase of immature rat bone in FE study.

^cdetermined via static analysis, cf. S1 Table.

^dLeong & Morgan 2008 [36], obtained by nanoindentation on rat fracture callus.

^eSimon *et al.*, 2011 [18], used in linear elastic FE model approach.

doi:10.1371/journal.pone.0115695.t002

Evaluation and corroboration of the numerical fracture healing model

The simulations of *in vivo* rat studies from literature showed good agreement for several combinations of fixation stiffness and fracture gap size qualitatively (successful healing or not) and quantitatively (direct comparison of the simulated and the *ex vivo* measured callus stiffness at a specific time point – Fig. 5). However, some large differences exist (Table 1). First, at large fracture gap sizes (3 mm & 5 mm), a successful healing process with high callus stiffness was

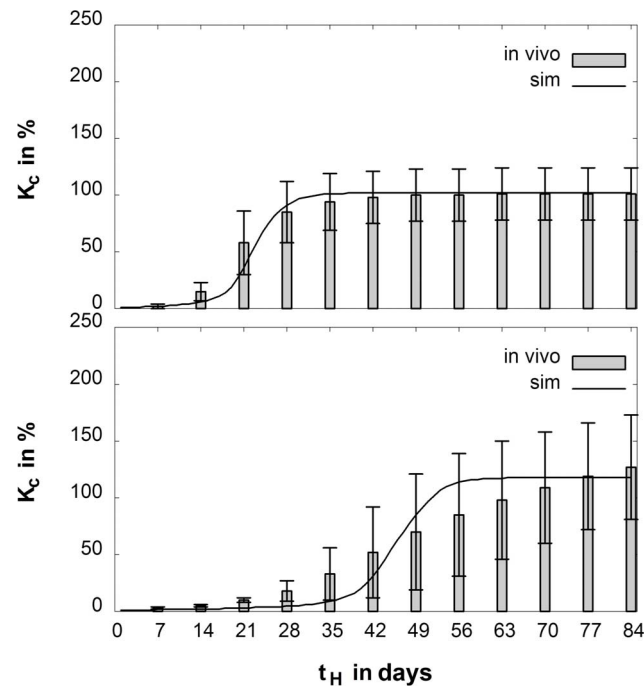


Fig. 3. Course of callus stiffness (K_c) over the healing time (t_H) under rigid (top) and flexible (bottom) fixation. Bars indicate *in vivo* data (statistical means and 95% confidence intervals) from the rat experiment [29], that was used to calibrate the numerical model, solid line represents the outcome of the numerical simulation after calibration.

doi:10.1371/journal.pone.0115695.g003

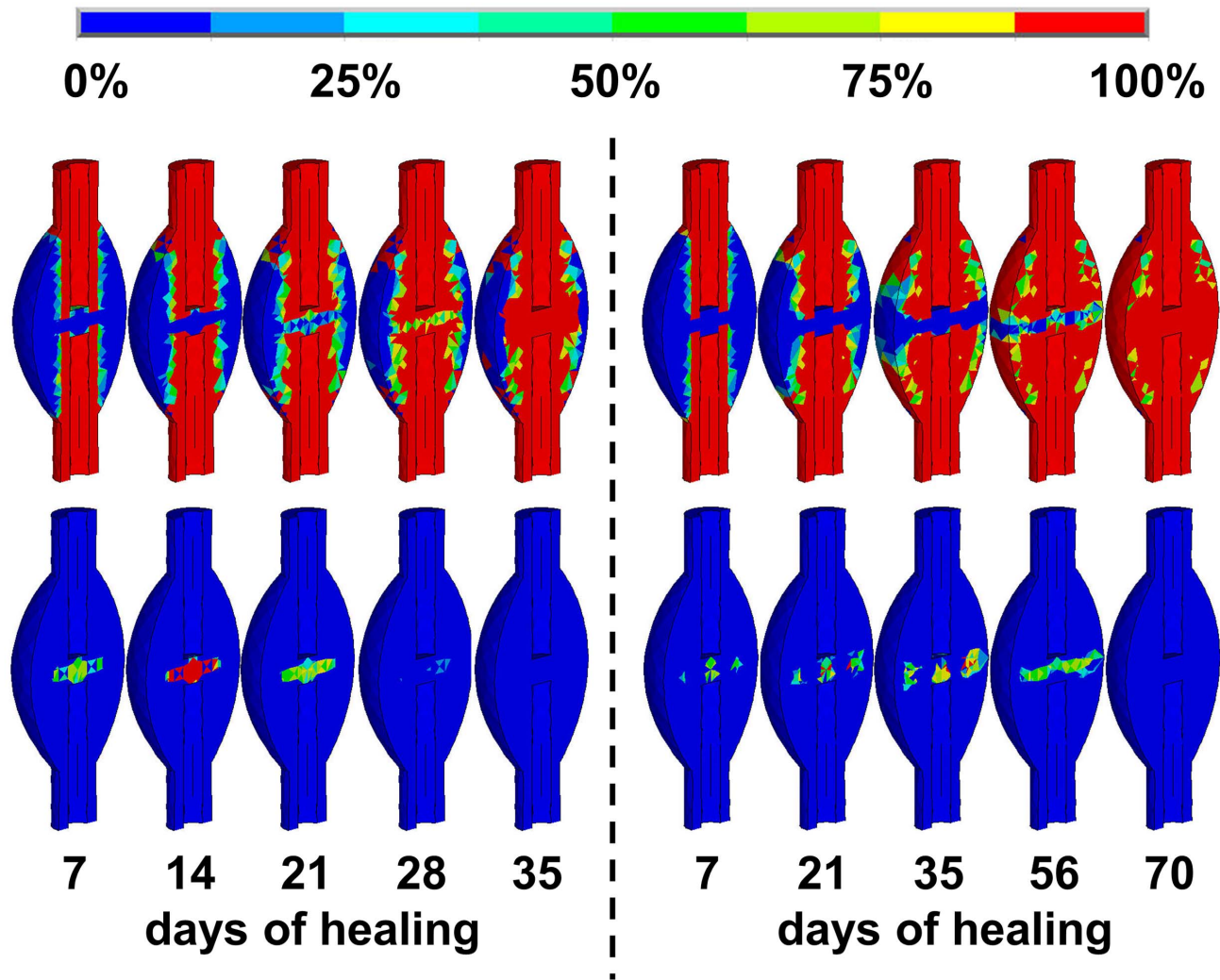


Fig. 4. Concentration (tissue type fraction within each finite element) of bone (top) and cartilage (bottom) over the healing time for the rigidly (left) and the flexibly (right) fixated animals.

doi:10.1371/journal.pone.0115695.g004

predicted, whereas there was no measureable callus stiffness observed *in vivo* [30, 31]. Second, a successful healing was simulated for old female rats after 42 days with a predicted callus stiffness of 107%, whereas the *ex vivo* measured callus stiffness was still low at $25 \pm 9\%$ [3]. Furthermore, the simulated stiffness of fracture calluses, which are completely filled with woven bone, were in some cases lower [3, 5, 30] (differences up to 76% of intact bone stiffness) or higher [1] (differences up to 47% of intact bone stiffness) than the measured *in vivo* results (Table 1).

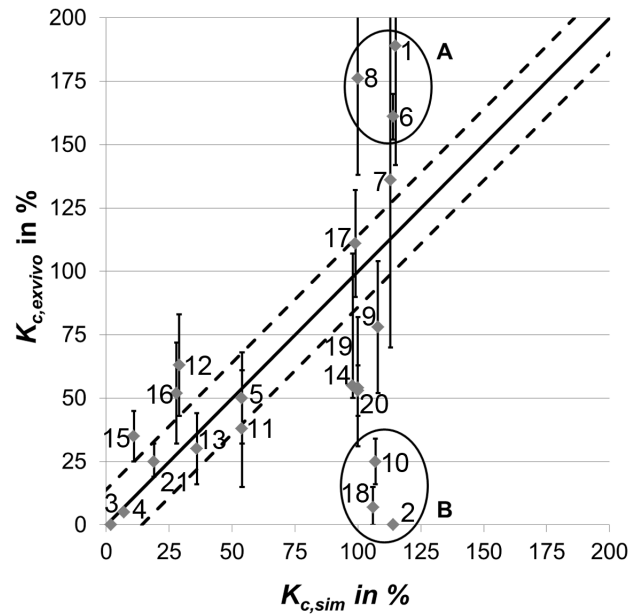


Fig. 5. Comparison of simulated ($K_{c,sim}$) and *ex vivo* measured ($K_{c,exvivo}$) callus stiffness of experimental studies from literature. The points and error bars indicate mean and standard deviations or median and interquartile ranges. Numbers of the single *in vivo* data points refer to Table 1. The solid line represents perfect agreement and the dashed lines indicate uncertainty ranges of the simulations due to variations in gap size, free bending length of the pins, and bodyweight of the rats ($\pm 14\%$ of the intact bone stiffness, determined in a preceded sensitivity analysis as described in the discussion section). In some cases, numerical predictions clearly underestimated the callus stiffness after bony bridging (group A) and in some cases, successful healing with high callus stiffness was predicted although no healing was observed *in vivo* and low callus stiffness was measured *ex vivo* (group B).

doi:10.1371/journal.pone.0115695.g005

Prediction of callus stiffness subject to bodyweight, fixation stiffness and fracture gap size

Using fit curves with a sigmoidal shape, the simulated course of callus stiffness over the healing time could be replicated well with a maximal error of $<5\%$ of the intact bone stiffness (cf. S2 Table, which provides fit curve parameters for numerous different combinations of bodyweight, fixation stiffness and fracture gap size). The time to heal (assumed to be the time point when the callus stiffness reached 90% of the intact bone stiffness) was prolonged for larger gap sizes, lower fixation stiffness and higher bodyweights of the rats (Fig. 6).

Discussion

In this study, a simplified version of an already existing fracture healing algorithm was successfully adapted to the healing process in rats by calibrating the thresholds of the underlying mechanoregulatory tissue differentiation rules. To simulate the time course of the callus stiffness and the patterns of bone and cartilage formation according to *in vivo* findings in rats [2, 29], the threshold values of the mechanical stimuli (volumetric and distortional strains) had to be shifted towards higher load

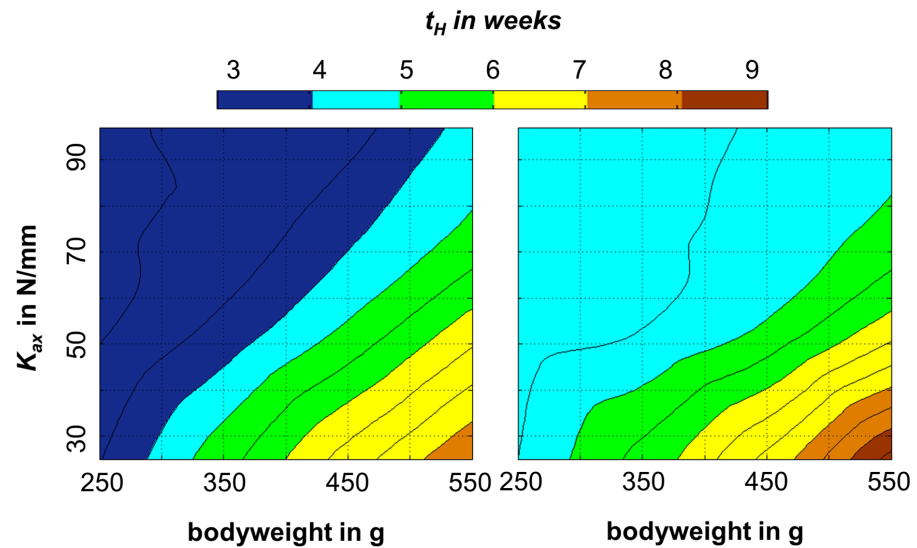


Fig. 6. Time to heal (t_H , defined as time point, when callus stiffness reached 90% of intact bone stiffness) in relation to bodyweight of the rats and axial stiffness (K_{ax}) of the external fixator at a fracture gap size of 1 mm (left) and 2 mm (right), calculated using the parameters given in supplemental material (cf. [S2 Table](#)).

doi:10.1371/journal.pone.0115695.g006

levels, which is in contrast to the simulations of Checa and colleagues [22]. In their study, the mechanical conditions to allow bone formation had to be shifted towards higher load levels for the sheep. However, the authors used a different numerical model for simulating the healing processes and used a different *in vivo* dataset for evaluating the simulations. Due to the differences of both numerical models (Checa *et al.* used a poroelastic description of the material properties, and a linear combination of the fluid flow and the distortional strain as mechanical stimulus and simulated several cell activities such as migration and proliferation), it is hard to directly compare their simulation results with the findings of this study. Therefore, it remains unclear if the differences in the necessary adaptation of the load levels from the sheep to the rat are due to differences between either the numerical models or the *in vivo* data used for evaluation. Further simulations with both models using the same *in vivo* data are required to clarify this issue.

In the present study, several published *in vivo* studies using rats were simulated to test the validity of the applied algorithm for other combinations of the experimental parameters bodyweight, fixation stiffness and fracture gap size (Table 1). With the exception of healing scenarios in which the healing process was seemingly more influenced by biological factors (large fracture gaps [30, 31] and age [3]), the achieved numerical predictions agreed particularly well with the respective *in vivo* findings (Table 1). Taking the variations of the *ex vivo* measured callus stiffness into account, which showed standard deviations of up to 47% [30] and interquartile ranges of 139% [32] of the intact bone stiffness, there were only

6 of 21 cases showing a considerable mismatch between simulations and *in vivo* data.

A preceding sensitivity study using the calibrated numerical model showed that varying the gap size by 0.1 mm, the offset of the fixator body by 0.5 mm, and the bodyweight by 25 g (all standard deviations) led to standard deviations of up to 14% for the rigid group and up to 20% for the flexible group and a maximum range of the callus stiffness of up to 57% (rigid) and up to 77% (flexible) of the intact bone stiffness ([S1 Fig.](#)). Aside from biological differences between the rats, which also have an influence on the healing process, these simulation results explain variations of the *ex vivo* measured callus stiffness due to variations of experimental parameters. For example, the range of the bodyweight of the rats used in the study of Mark *et al.* [5] was 350 to 450 g. Simulating the healing process with a bodyweight of 400 g led to a difference of 45% of the intact bone stiffness at the 6 weeks healing time point ($50 \pm 18\%$ [5] vs. 95%) whereas this difference was minimal ($50 \pm 18\%$ [5] vs. 52%), when the healing process was simulated with 450 g bodyweight ([Table 1](#)) indicating a good agreement of the achieved numerical predictions considering variations in the experimental parameters.

However, there were several necessary assumptions and simplifications that were made. Firstly, material behavior was simplified to linear elastic, isotropic behavior. In particular, this limits the model outcomes in the first phases of healing when tissues are still very flexible and show a distinct fluid phase. Secondly, the adjusted rules for tissue differentiation are simplified to a minimum, compared to previous numerical simulation studies of this group [18, 19, 33, 34] and completely focus on mechanoregulation without considering any biological influences. Thirdly, as previously mentioned, the predictions for healing processes accompanied by large fracture gaps (3 & 5 mm) did not fit well to the *in vivo* results ([Table 1](#)). Enlarging the fracture gap in the applied numerical model leads to a delayed healing since it takes longer to bridge the fracture gap with the same rate of bone formation ([S2 Table](#)). However, as long as this bone formation rate will not be set to zero and the IFM will be high enough to prevent a mechanical understimulation of the callus tissue, the model will predict successful healing for all gap sizes. This suggested that the causality of a critical size defect cannot be explained by mechanical stimuli solely and that biological factors must be considered. To include the simulation of non-unions in this model as well, the bone formation rate could be described as a function of the healing time. Thereby a decay of the biological factors promoting tissue development over the healing time could be incorporated allowing the simulation of non-unions as well. Since the exact, underlying biological mechanisms are, so far, not known to predict the tissue development in those cases, the present simulations were focused on the influence of the biomechanical factors on the healing process.

In conclusion, the present numerical model was considered valid for normal healing processes of transverse osteotomies in rats with fracture gap sizes in the range of 0.5 to 2 mm and bodyweights in the range of 250 to 550 g, stabilized by

external fixators with an axial fixation stiffness in the range of 10 to 119 N/mm. The data presented in this study might help to improve new investigations of fracture healing in rats by predicting the time course of the healing process prior to the animal studies and allowing the transfer of new *in vivo* findings to previous studies with different bodyweight, fixation stiffness and fracture gap sizes.

Supporting Information

S1 Fig. Course of callus stiffness (KC) over the healing time (tH) under rigid and flexible fixation.

[doi:10.1371/journal.pone.0115695.s001](https://doi.org/10.1371/journal.pone.0115695.s001) (PDF)

S1 Table. Bending stiffness calculated with the three finite element models in relation to the Young's moduli of the different tissue types.

[doi:10.1371/journal.pone.0115695.s002](https://doi.org/10.1371/journal.pone.0115695.s002) (PDF)

S2 Table. Parameters of the sigmoid function (a , b , t_0 - cf. [equation 4](#)), used to predict the time course of the callus stiffness (Kc) in percent (%) of the intact bones under different combinations of BW , Kax , and Sfr .

[doi:10.1371/journal.pone.0115695.s003](https://doi.org/10.1371/journal.pone.0115695.s003) (PDF)

Author Contributions

Conceived and designed the experiments: TW MS AI LC. Performed the experiments: TW MS. Analyzed the data: TW MS. Contributed reagents/materials/analysis tools: TW MS AI LC. Wrote the paper: TW MS LC.

References

1. Claes L, Blakytyn R, Gockelmann M, Schoen M, Ignatius A, et al. (2009) Early Dynamization by Reduced Fixation Stiffness Does Not Improve Fracture Healing in a Rat Femoral Osteotomy Model. *J Orthop Res* 27: 22–27.
2. Recknagel S, Bindi R, Kurz J, Wehner T, Ehrnthaller C, et al. (2011) Experimental blunt chest trauma impairs fracture healing in rats. *J Orthop Res* 29: 734–739.
3. Strube P, Sentuerk U, Riha T, Kaspar K, Mueller M, et al. (2008) Influence of age and mechanical stability on bone defect healing: age reverses mechanical effects. *Bone* 42: 758–764.
4. Strube P, Mehta M, Baerenwaldt A, Trippens J, Wilson CJ, et al. (2009) Sex-specific compromised bone healing in female rats might be associated with a decrease in mesenchymal stem cell quantity. *Bone* 45: 1065–1072.
5. Mark H, Rydevik B (2005) Torsional stiffness in healing fractures: Influence of ossification. An experimental study in rats. *Acta orthopaedica* 76: 428–433.
6. Claes L, Augat P, Suger G, Wilke HJ (1997) Influence of size and stability of the osteotomy gap on the success of fracture healing. *J Orthop Res* 15: 577–584.
7. Einhorn TA (1998) The cell and molecular biology of fracture healing. *Clin Orthop Relat Res*: S7–S21.
8. Goodship AE, Kenwright J (1985) The influence of induced micromovement upon the healing of experimental tibial fractures. *J Bone Joint Surg Br* 67: 650–655.
9. Claes LE, Heigele CA (1999) Magnitudes of local stress and strain along bony surfaces predict the course and type of fracture healing. *J Biomech* 32: 255–266.

10. **Prendergast PJ, Huiskes R, Soballe K** (1997) ESB Research Award 1996. Biophysical stimuli on cells during tissue differentiation at implant interfaces. *J Biomech* 30: 539–548.
11. **Wehner T, Wolfram U, Henzler T, Niemeyer F, Claes L, et al.** (2010) Internal forces and moments in the femur of the rat during gait. *J Biomech* 43: 2473–2479.
12. **Isaksson H, van Donkelaar CC, Huiskes R, Ito K** (2008) A mechano-regulatory bone-healing model incorporating cell-phenotype specific activity. *J Theor Biol* 252: 230–246.
13. **Bailón-Plaza A, Van Der Meulen MCH** (2001) A Mathematical Framework to Study the Effects of Growth Factor Influences on Fracture Healing. *J Theor Biol* 212: 191–209.
14. **Checa S, Prendergast PJ** (2009) A Mechanobiological Model for Tissue Differentiation that Includes Angiogenesis: A Lattice-Based Modeling Approach. *Annals of Biomedical Engineering* 37: 129–145.
15. **Geris L, Sloten JV, Van Oosterwyck H** (2010) Connecting biology and mechanics in fracture healing: an integrated mathematical modeling framework for the study of nonunions. *Biomech Model Mechanobiol* 9: 713–724.
16. **Gomez-Benito MJ, Garcia-Aznar JM, Kuiper JH, Doblare M** (2005) Influence of fracture gap size on the pattern of long bone healing: a computational study. *J Theor Biol* 235: 105–119.
17. **Lacroix D, Prendergast PJ** (2002) A mechano-regulation model for tissue differentiation during fracture healing: analysis of gap size and loading. *J Biomech* 35: 1163–1171.
18. **Simon U, Augat P, Utz M, Claes L** (2011) A numerical model of the fracture healing process that describes tissue development and revascularisation. *Comput Methods Biomech Biomed Engin* 14: 79–93.
19. **Steiner M, Claes L, Ignatius A, Niemeyer F, Simon U, et al.** (2013) Prediction of fracture healing under axial loading, shear loading and bending is possible using distortional and dilatational strains as determining mechanical stimuli. *J R Soc Interface* 10: 20130389.
20. **Wehner T, Claes L, Ignatius A, Simon U** (2012) Optimization of intramedullary nailing by numerical simulation of fracture healing. *J Orthop Res* 30: 569–573.
21. **Wehner T, Claes L, Niemeyer F, Nolte D, Simon U** (2010) Influence of the fixation stability on the healing time—a numerical study of a patient-specific fracture healing process. *Clin Biomech* 25: 606–612.
22. **Checa S, Prendergast PJ, Duda GN** (2011) Inter-species investigation of the mechano-regulation of bone healing: Comparison of secondary bone healing in sheep and rat. *J Biomech* 44: 1237–1245.
23. **Oni OO, Dunning J, Mobbs RJ, Gregg PJ** (1991) Clinical factors and the size of the external callus in tibial shaft fractures. *Clin Orthop Relat Res* 273: 278–283.
24. **Shelfbine SJ, Augat P, Claes L, Simon U** (2005) Trabecular bone fracture healing simulation with finite element analysis and fuzzy logic. *J Biomech* 38: 2440–2450.
25. **Rubin CT, Lanyon LE** (1987) Osteoregulatory nature of mechanical stimuli: Function as a determinant for adaptive remodeling in bone. *J Orthop Res* 5: 300–310.
26. **Wehner T, Gruchenberg K, Bindl R, Recknagel S, Steiner M, et al.** (2014) Temporal delimitation of the healing phases via monitoring of fracture callus stiffness in rats. *Journal of Orthopaedic Research* 32: 1589–1595.
27. **Recknagel S, Bindl R, Kurz J, Wehner T, Schoengraf P, et al.** (2012) C5aR-antagonist significantly reduces the deleterious effect of a blunt chest trauma on fracture healing. *J Orthop Res* 30: 581–586.
28. **Recknagel S, Bindl R, Wehner T, Göckelmann M, Wehrle E, et al.** (2013) Conversion from external fixator to intramedullary nail causes a second hit and impairs fracture healing in a severe trauma model. *J Orthop Res* 31: 465–471.
29. **Wehner T, Gruchenberg K, Bindl R, Recknagel S, Steiner M, et al.** (2014) Temporal Delimitation of the Healing Phases via Monitoring of Fracture Callus Stiffness in Rats. *J Orthop Res*: in press.
30. **Harrison LJ, Cunningham JL, Stromberg L, Goodship AE** (2003) Controlled induction of a pseudarthrosis: A study using a rodent model. *J Orthop Trauma* 17: 11–21.
31. **Mehta M, Schell H, Schwarz C, Peters A, Schmidt-Bleek K, et al.** (2011) A 5-mm femoral defect in female but not in male rats leads to a reproducible atrophic non-union. *Arch Orthop Trauma Surg* 131: 121–129.

32. **Kaspar K, Schell H, Toben D, Matziolis G, Bail HJ** (2007) An easily reproducible and biomechanically standardized model to investigate bone healing in rats, using external fixation. *Biomedizinische Technik* 52: 383–390.
33. **Steiner M, Claes L, Ignatius A, Simon U, Wehner T** (2014) Disadvantages of interfragmentary shear on fracture healing—mechanical insights through numerical simulation. *J Orthop Res* 32: 865–872.
34. **Steiner M, Claes L, Ignatius A, Simon U, Wehner T** (2014) Numerical simulation of callus healing for optimization of fracture fixation stiffness. *PLoS One* 9: e101370.
35. **Smit TH, Huyghe JM, Cowin SC** (2002) Estimation of the poroelastic parameters of cortical bone. *J Biomech* 35: 829–835.
36. **Leong PL, Morgan EF** (2008) Measurement of fracture callus material properties via nanoindentation. *Acta Biomaterialia* 4: 1569–1575.
37. **Mehta M, Duda GN, Perka C, Strube P** (2011) Influence of Gender and Fixation Stability on Bone Defect Healing in Middle-aged Rats: A Pilot Study. *Clin Orthop Relat Res* 469: 3102–3110.